Transition Metal Chemistry
https://doi.org/10.1007/s11243-019-00339-x

Synthesis and characterization of diiron ethane-1,2-dithiolate complexes with tricyclohexylphosphine, methyl diphenylphosphinite, or tris(2-thienyl)phosphine coligands

Lin Yan[1] · Ao Li[2] · Qi-Min Xiao[2] · Xu-Feng Liu[1] · Yu-Long Li[2] · Zhong-Qing Jiang[3] · Hong-Ke Wu[4]

Received: 11 January 2019 / Accepted: 15 June 2019

Abstract

We have prepared three diiron ethane-1,2-dithiolate complexes $[Fe_2(CO)_5L(\mu\text{-}SCH_2CH_2S)]$ [$L = P(C_6H_{11})_3$, **2**; Ph_2POCH_3, **3**; $P(2\text{-}C_4H_3S)_3$, **4**] by CO exchange of the starting complex $[Fe_2(CO)_6(\mu\text{-}SCH_2CH_2S)]$ (**1**) with the corresponding phosphine ligands tricyclohexylphosphine, methyl diphenylphosphinite, or tris(2-thienyl)phosphine in the presence of Me_3NO as an oxidant for CO. The complexes have been characterized by elemental analysis, spectroscopy, and single-crystal X-ray diffraction analysis.

Introduction

Since the initial characterization of the active site of [FeFe]-hydrogenases [1–5], much effort has been devoted to the design and synthesis of a large number of diiron complexes of the general formula $[Fe_2(CO)_{6-n}(L)_n(\mu\text{-}SRS)]$ ($n = 0$–6) in order to mimic the structural and functional attributes of these enzymes. [FeFe]-hydrogenases are efficient catalysts for the reduction of protons to H_2 which is a promising source of clean energy [6–8]. X-ray crystallographic studies have revealed that the active site of [FeFe]-hydrogenases consists of a diiron cluster with a bridging dithiolate cofactor, also ligated by carbonyls, cyanides, and a cysteinyl ligand connected to a tetrairon cluster [9, 10]. FTIR [11] and density functional theory (DFT) [12] studies have confirmed that the bridging dithiolate cofactor is 2-azapropane-1,3-dithiolate and furthermore that the nitrogen atom plays a significant role in shuttling protons to and from the iron atoms [13]. Guided by this structural information, a great number of diiron azadithiolate complexes of general formula $[Fe_2(CO)_6\{\mu\text{-}SCH_2N(R)CH_2S\}]$ have been prepared and characterized in recent decades [14–17]. In addition, alternative ligands such as cyanides [18], phosphines [19], thioethers [20], and *N*-heterocyclic carbenes (NHC) [21] have also been introduced, in order to mimic the ligands at the active site of these enzymes.

The diiron ethane-1,2-dithiolate complex $[Fe_2(CO)_6(\mu\text{-}SCH_2CH_2S)]$ (**1**) was reported more than 30 years ago [22], being prepared by heating $Fe_3(CO)_{12}$ with 1,2-ethanedithiol in toluene solution. The reactions of complex **1** with other ligands have been widely studied, due to its structural similarity with the diiron propane-1,3-dithiolate complex $[Fe_2(CO)_6(\mu\text{-}SCH_2CH_2CH_2S)]$ [23, 24]. In continuation of our ongoing interests in diiron chemistry, we have investigated the synthesis of some diiron ethane-1,2-dithiolate complexes by CO exchange of the parent complex **1** with phosphine ligands. We believe that such phosphine ligands can mimic the cyanides found in the active site of [FeFe]-hydrogenases. In this contribution, we report the synthesis and characterization of three diiron ethane-1,2-dithiolate complexes with tricyclohexylphosphine, methyl diphenylphosphinite, or tris(2-thienyl)phosphine coligands, together with their X-ray crystal structures.

✉ Xu-Feng Liu
nkxfliu@126.com

1 School of Materials and Chemical Engineering, Ningbo University of Technology, Ningbo 315211, China

2 College of Chemistry and Environmental Engineering, Sichuan University of Science and Engineering, Zigong 643000, China

3 Department of Physics, Key Laboratory of ATMMT Ministry of Education, Zhejiang Sci-Tech University, Hangzhou 310018, China

4 College of Chemical Engineering, Zhejiang University of Technology, Hangzhou 310014, China

Published online: 21 June 2019

Experimental

Tricyclohexylphosphine, methyl diphenylphosphinite, tris(2-thienyl)phosphine, and $Me_3NO{\cdot}2H_2O$ were commercial products that were used as received. Complex **1** was prepared according to the literature procedure [22]. IR spectra were recorded on a Nicolet MAGNA 560 FTIR spectrometer. ^{1}H, ^{31}P{^{1}H}, ^{13}C{^{1}H} NMR spectra were obtained on a Bruker Avance 500 MHz spectrometer. Elemental analyses were obtained with a Perkin-Elmer 240C analyzer.

Synthesis of $[Fe_2(CO)_5\{P(C_6H_{11})_3\}(\mu\text{-}SCH_2CH_2S)]$ (2)

To a solution of $[Fe_2(CO)_6(\mu\text{-}SCH_2CH_2S)]$ (0.037 g, 0.1 mmol) and tricyclohexylphosphine (0.028 g, 0.1 mmol) in CH_2Cl_2 (5 mL) was added a solution of $Me_3NO{\cdot}2H_2O$ (0.011 g, 0.1 mmol) in MeCN (5 mL). The mixture was stirred at room temperature for 1 h, and then, the solvent was reduced on a rotary evaporator. The residue was subjected to TLC using CH_2Cl_2/petroleum ether = 1:3 (v/v) as eluent. From the main red band, 0.042 g (68%) of complex **2** was obtained as a red solid. IR (CH_2Cl_2, cm^{-1}): $\nu_{C\equiv O}$ 2043 (vs), 1977 (vs), 1921 (m). ^{1}H NMR (500 MHz, $CDCl_3$): 2.27–2.18 (m, 4H, Cy*H*), 2.06–2.03 (m, 6H, Cy*H*, and SCH_2), 1.92–1.91 (m, 6H, Cy*H*, and SCH_2), 1.83–1.77 (m, 6H, Cy*H*), 1.55–1.47 (m, 6H, Cy*H*), 1.32–1.26 (m, 9H, Cy*H*) ppm. ^{31}P{^{1}H} NMR (200 MHz, $CDCl_3$, 85% H_3PO_4): 71.57 (s) ppm. ^{13}C{^{1}H} NMR (125 MHz, $CDCl_3$): 216.90 (d, J_{P-C} = 10.5 Hz, PFe*C*O), 210.71 (Fe*C*O), 38.38 (d, J_{P-C} = 16.4 Hz, Cy*C*), 30.18 (Cy*C*), 36.31 (S*C*H$_2$), 27.89 (d, J_{P-C} = 9.9 Hz, Cy*C*), 26.42 (Cy*C*) ppm. Anal. Calcd. for $C_{25}H_{37}Fe_2O_5PS_2$: C, 48.09; H, 5.97. Found: C, 48.28; H, 6.19%.

Synthesis of $[Fe_2(CO)_5(Ph_2POCH_3)(\mu\text{-}SCH_2CH_2S)]$ (3)

The procedure was similar to that for complex **2**, except that methyl diphenylphosphinite (0.022 g, 0.1 mmol) was used instead of tricyclohexylphosphine; 0.039 g (70%) of complex **3** was obtained as a red solid. IR (CH_2Cl_2, cm^{-1}): $\nu_{C\equiv O}$ 2046 (vs), 1987 (vs), 1935 (m). ^{1}H NMR (500 MHz, $CDCl_3$): 7.71 (s, 4H, Ph*H*), 7.47 (s, 6H, Ph*H*), 3.59 (d, J = 11 Hz, 3H, C*H*$_3$), 2.01 (s, 2H, SC*H*$_2$), 1.73 (s, 2H, SC*H*$_2$) ppm. ^{31}P{^{1}H} NMR (200 MHz, $CDCl_3$, 85% H_3PO_4): 168.07 (s) ppm. Anal. Calcd. for $C_{20}H_{17}Fe_2O_6PS_2$: C, 42.89; H, 3.06. Found: C, 42.68; H, 3.14%.

Synthesis of $[Fe_2(CO)_5\{P(2\text{-}C_4H_3S)_3\}(\mu\text{-}SCH_2CH_2S)]$ (4)

The procedure was similar to that for complex **2**, except that tris(2-thienyl)phosphine (0.028 g, 0.1 mmol) was used instead of tricyclohexylphosphine; 0.045 g (73%) of complex **4** was obtained as a red solid. IR (CH_2Cl_2, cm^{-1}): $\nu_{C\equiv O}$ 2048 (vs), 1991 (vs), 1943 (m). ^{1}H NMR (500 MHz, $CDCl_3$): 7.67 (s, 3H, thienyl*H*), 7.53 (s, 3H, thienyl*H*), 7.17 (s, 3H, thienyl*H*), 2.06 (d, J = 8 Hz, 2H, SC*H*$_2$), 1.63 (d, J = 8 Hz, 2H, SC*H*$_2$) ppm. ^{31}P{^{1}H} NMR (200 MHz, $CDCl_3$, 85% H_3PO_4): 30.26 (s) ppm. Anal. Calcd. for $C_{19}H_{13}Fe_2O_5PS_5$: C, 36.56; H, 2.10. Found: C, 36.31; H, 2.28%.

X-ray crystal structure determination

A single crystal of each complex was mounted on a Bruker D8 QUEST diffractometer. Data were collected at 296(2) K using a graphite monochromator with MoKα radiation (λ = 0.71073 Å) in the ω–ϕ scanning mode. Data collection and reduction were accomplished with APEX2 software [25]. Absorption corrections were made with the SADABS program [26]. Using OLEX2 [27], the structure was solved by direct methods using the SHELXS program [28] and refined by full-matrix least-squares techniques on F^2. Hydrogen atoms were located using geometric methods. Details of crystal data, data collections, and structure refinements are summarized in Table 1.

Electrochemical experiments

The electrochemical properties of complexes **2**–**4** were studied by cyclic voltammetry (CV) in MeCN solution. Electrochemical measurements were taken under nitrogen using a CHI 620 Electrochemical work station. The supporting electrolyte n-Bu_4NPF_6 was recrystallized several times from CH_2Cl_2 solution by the addition of hexane. CV scans were obtained in a three-electrode cell with a glassy carbon electrode (3 mm diameter) as the working electrode, a platinum wire as the counter electrode, and a nonaqueous Ag/Ag^+ electrode as the reference electrode. The potential scale was calibrated against the Fc/Fc^+ couple, and all values are reported versus this reference.

Results and discussion

Synthesis and characterization of complexes 2–4

The synthetic route to complexes **2**–**4** is shown in Scheme 1. Treatment of the starting complex **1** with one equivalent of the corresponding phosphine ligand tricyclohexylphosphine, methyl diphenylphosphinite, or tris(2-thienyl)phosphine in the presence of Me_3NO as an oxidant for CO afforded the target complexes in satisfactory yields. All three complexes are air-stable red solids, soluble in medium-polarity solvents such as CH_2Cl_2 and THF.

Table 1 Crystal data and structure refinements details for the complexes **2**–**4**

Complex	**2**	**3**	**4**
Empirical formula	$C_{25}H_{37}Fe_2O_5PS_2$	$C_{20}H_{17}Fe_2O_6PS_2$	$C_{19}H_{13}Fe_2O_5PS_5$
Formula weight	624.33	560.12	624.26
Temperature (K)	296(2)	296(2)	296(2)
Crystal system	Monoclinic	Orthorhombic	Triclinic
Space group	$P2_1/n$	Pbca	P-1
a (Å)	11.7852(6)	16.3721(7)	9.2969(4)
b (Å)	11.7247(6)	15.7473(7)	10.4370(4)
c (Å)	21.7489(12)	17.8364(8)	13.4614(6)
α (°)	90	90	88.5670(10)
β (°)	103.700(2)	90	75.6860(10)
γ (°)	90	90	72.6510(10)
V (Å^3)	2919.7(3)	4598.5(4)	1206.38(9)
Z	4	8	2
D_{calc} (g cm^{-3})	1.420	1.618	1.719
μ (mm^{-1})	1.223	1.547	1.731
F(000)	1304.0	2272.0	628.0
Crystal size (mm^3)	0.3×0.2×0.18	0.32×0.22×0.18	0.2×0.2×0.2
Radiation	MoKα (λ = 0.71073)	MoKα (λ = 0.71073)	MoKα (λ = 0.71073)
2θ range (°)	4.43–61.512	4.254–50.226	4.742–55.172
hkl range	$-16 \le h \le 16$ $-16 \le k \le 16$ $-31 \le l \le 31$	$-19 \le h \le 18$ $-18 \le k \le 18$ $-21 \le l \le 21$	$-12 \le h \le 12$ $-13 \le k \le 13$ $-17 \le l \le 17$
Reflections collected	96939	90360	51965
Independent reflections	8453 [R_{int} = 0.0427]	4099 [R_{int} = 0.0484]	5518 [R_{int} = 0.0297]
Data/restraints/parameters	8453/0/316	4099/0/281	5518/18/289
Goodness of fit on F^2	1.029	1.185	1.062
Final *R* indexes ($I > 2\sigma(I)$)	0.0357/0.0769	0.0244/0.0657	0.0761/0.2307
Final R indexes (all data)	0.0603/0.0847	0.0362/0.0793	0.0798/0.2355
Largest diff peak and hole/e Å^{-3}	0.40/−0.34	0.46/−0.48	2.35/−1.37

Scheme 1 Synthesis of the complexes **2**–**4**

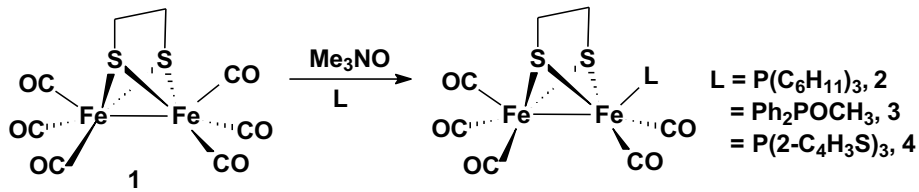

The IR spectra of complexes **2**–**4** each show three absorption bands in the region of 2048–1921 cm^{-1}, which can be assigned to the stretching vibrations of the terminal carbonyl ligands, close to those of analogous complexes [29]. The ν(C≡O) values are redshifted compared to those of the parent complex **1** (2079, 2039, 2009, 1996 cm^{-1}) [22] as well as other all-carbonyl complexes [30], which is expected since the phosphine ligands are more strongly electron donating than CO [31]. The ^{1}H NMR spectrum of complex **3** displays two singlets at 2.01 and 1.73 ppm for the methylene protons, whereas the ^{1}H NMR spectrum of complex **4** shows two doublets at 2.06 and 1.63 ppm for the corresponding protons, probably due to the different steric effects of the phosphine coligand. The ^{31}P{^{1}H} NMR spectra of complexes **2** and **4** each show single resonances at 71.57 and 30.26 ppm, respectively, similar to those of some phosphine-substituted diiron analogues [32, 33], but significantly larger than those of the corresponding free phosphines. Meanwhile, the ^{31}P{^{1}H} NMR spectrum of complex **3** exhibits a single resonance at 168.07 ppm, notably different to those of complexes **2** and **4** because of the P–O bond in complex **3**, but consistent with the complex [$Fe_2(CO)_5${P(OEt)$_3$}(μ-SCH$_2$CH$_2$CH$_2$S)] (171.09 ppm) [19]. The ^{13}C{^{1}H} NMR spectrum of complex **2** shows a doublet at 216.90 ppm with a coupling constant

$J_{P-C} = 10.5$ Hz for the terminal carbonyls of the $PFe(CO)_2$ moiety, plus a singlet at 210.71 ppm for the terminal carbonyls of the $Fe(CO)_3$ unit.

X-ray crystal structures of complexes 2–4

In order to determine the structures of the complexes, X-ray quality crystals were obtained by slow evaporation of CH_2Cl_2/hexane solutions at 4 °C and analyzed by X-ray diffraction analysis. The ORTEP views are shown in Figs. 1, 2, and 3, and selected geometric data are listed in Table 2. Complex **2** crystallizes in monoclinic space group $P2_1/n$ with four molecules in the unit cell and one molecule in the asymmetric unit. As shown in Fig. 1, complex **2** contains a diiron unit, which is coordinated by a bridging ethane-1,2-dithiolate ligand, five terminal carbonyls, and a tricyclohexylphosphine ligand. The phosphorus atom of the latter is located in an apical position of the distorted octahedral Fe2 atom, similar to the related phosphine-containing diiron complexes $[Fe_2(CO)_5(Ph_2PCH_2Ph)(\mu\text{-}SCH_2CH_2S)]$ [34], $[Fe_2(CO)_5\{P(2\text{-}C_6H_4OCH_3)_3\}\{\mu\text{-}SCH_2CH(CH_2O_2CFc)\}]$ (Fc = ferrocenyl) [35], and $[Fe_2(CO)_5(PPh_3)(\mu\text{-}SCH_2CH_2CH_2S)]$ [19]. The Fe1–Fe2 bond distance [2.4909(3) Å] is slightly shorter than that

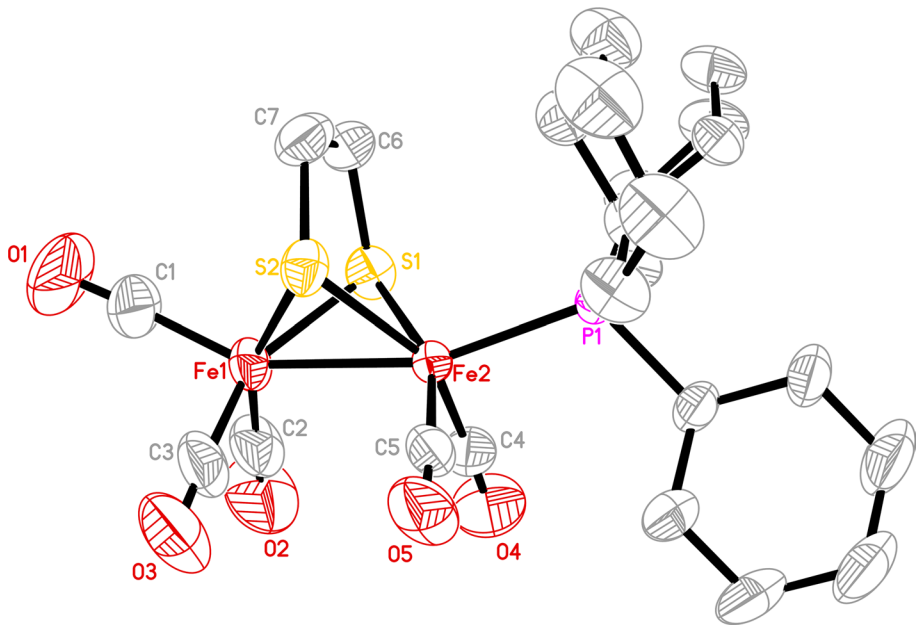

Fig. 1 ORTEP view of complex **2** with 50% probability level ellipsoids. Hydrogen atoms have been omitted for clarity

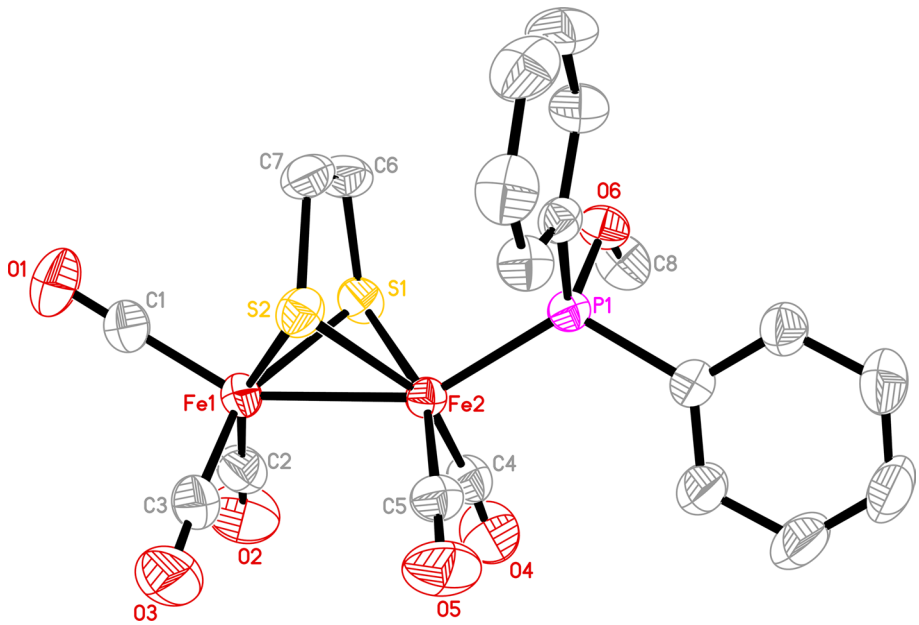

Fig. 2 ORTEP view of complex **3** with 50% probability level ellipsoids. Hydrogen atoms have been omitted for clarity

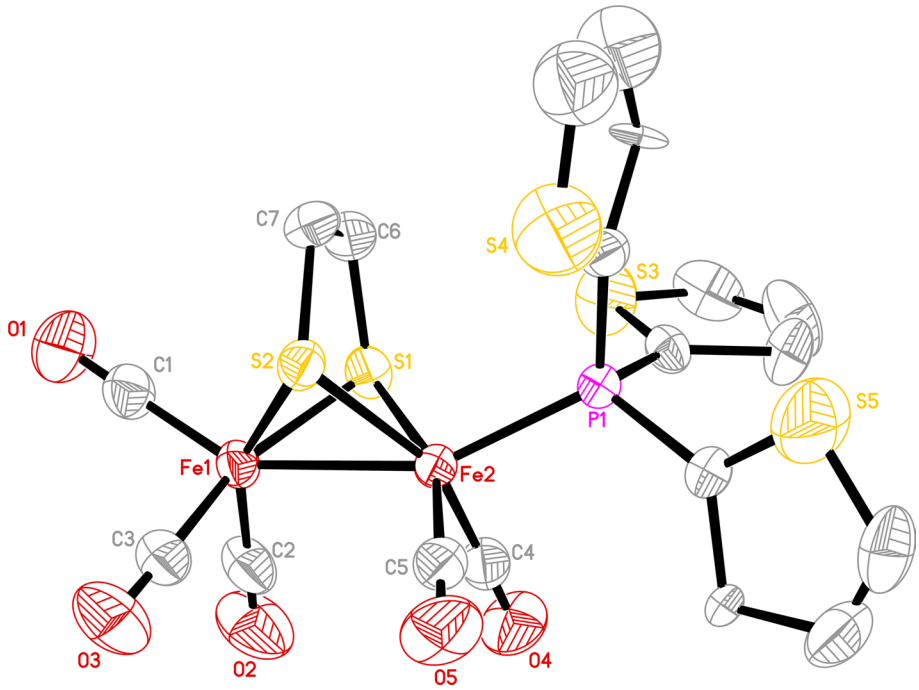

Fig. 3 ORTEP view of complex **4** with 50% probability level ellipsoids. Hydrogen atoms have been omitted for clarity

Table 2 Selected bond distances (Å) and angles (°) for the complexes **2**–**4**

Complex	**2**	**3**	**4**
Fe1–Fe2	2.4909(3)	2.5093(4)	2.5188(9)
Fe1–S1	2.2597(6)	2.2471(6)	2.2477(14)
Fe1–S2	2.2674(5)	2.2500(7)	2.2578(14)
Fe2–S1	2.2605(5)	2.2473(6)	2.2420(14)
Fe2–S2	2.2579(5)	2.2467(6)	2.2544(13)
Fe2–P1	2.2582(5)	2.2005(6)	2.2074(13)
S1–C6	1.826(2)	1.821(3)	1.832(6)
S2–C7	1.817(2)	1.825(3)	1.822(6)
C6–C7	1.492(3)	1.507(4)	1.530(9)
S1–Fe1–Fe2	56.575(14)	56.063(17)	55.77(4)
S1–Fe1–S2	79.291(19)	79.82(2)	79.75(5)
S2–Fe1–Fe2	56.420(14)	56.017(17)	56.00(4)
S1–Fe2–Fe1	56.545(15)	56.059(17)	55.98(4)
S2–Fe2–Fe1	56.786(14)	56.144(18)	56.13(4)
S2–Fe2–S1	79.47(2)	79.89(2)	79.94(5)
P1–Fe2–Fe1	160.337(17)	149.14(2)	153.65(4)
Fe1–S1–Fe2	66.880(16)	67.878(18)	68.25(4)
Fe2–S2–Fe1	66.794(16)	67.839(19)	67.87(4)
C7–C6–S1	112.58(14)	112.34(17)	112.6(4)
C6–C7–S2	112.11(15)	112.01(17)	111.0(4)

of complex **1** [2.505(2) Å] [36], showing that the tricyclohexylphosphine ligand does not appreciably affect the Fe–Fe bond. The Fe1–Fe2 bond distance is in fact notably shorter than that in natural [FeFe]-hydrogenases (2.55–2.62 Å) [9, 10]. The average Fe–C bond distance of the phosphine-substituted Fe (1.756 Å) is shorter than that of the unsubstituted Fe (1.784 Å), which can be attributed to the phosphine ligand having stronger electron-donating properties than CO [31]. The cyclohexyl rings of the tricyclohexylphosphine adopt a chair conformation in the crystal structure.

Complex **3** crystallizes in orthorhombic space group Pbca with eight molecules in the unit cell and one molecule in the asymmetric unit. As shown in Fig. 2, similar to complex **2**, complex **3** contains a diiron cluster with a bridging ethane-1,2-dithiolate ligand, plus five terminal carbonyls and an apically coordinated methyl diphenylphosphinite ligand. The Fe1–Fe2 bond distance [2.5093(4) Å] is slightly longer than that of complex **2**, but shorter than some diiron complexes with monophosphine [37] or diphosphine [38, 39] ligands.

Complex **4** crystallizes in triclinic space group P-1 with two molecules in the unit cell and one molecule in the asymmetric unit. As shown in Fig. 3, complex **4** consists of a diiron cluster with a bridging ethane-1,2-dithiolate ligand, plus five terminal carbonyls and an apically coordinated tris(2-thienyl)phosphine ligand. The Fe1–Fe2 bond distance [2.5188(9) Å] is longer than those of complexes **2** and **3**, suggesting that tris(2-thienyl)phosphine is more electron donating than tricyclohexylphosphine and methyl diphenylphosphinite.

Electrochemical studies

The electrochemical properties of complexes **2**–**4** were studied by CV in acetonitrile solution. The electrochemical data for the complexes **1**–**4** are listed in Table 3.

Table 3 Electrochemical data for the complexes **1**–**4**

Complex	E_{pc1} (V)	E_{pc2} (V)	E_{pa} (V)
1	−1.70	−2.11	+0.88
2	−1.97	–	+0.28
3	−1.94	−2.20	+0.42
4	−1.88	−2.10	+0.41

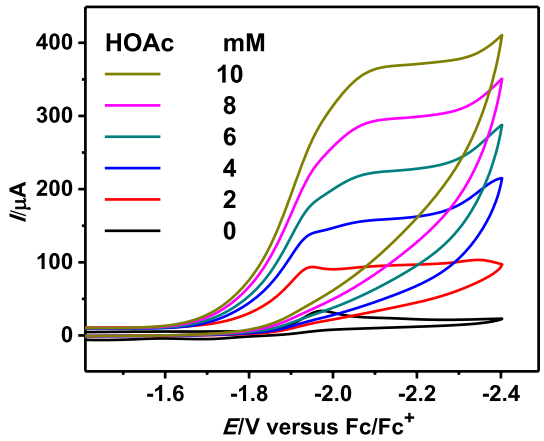

Fig. 4 Cyclic voltammogram of complex **2** (1.0 mM) with HOAc (0–10 mM) in 0.1 M n-Bu_4NPF_6/MeCN at a scan rate of 100 mV s^{-1}

Complex **2** shows a single irreversible reduction peak at −1.97 V, which can be ascribed to the reduction of Fe^IFe^I to Fe^IFe^0 [40]. This peak is shifted negatively by 0.27 V compared to the first reduction process of complex **1** (−1.70 V), reflecting the fact that the tricyclohexylphosphine ligand is more strongly electron donating than CO [31]. Meanwhile, complex **3** shows two irreversible reduction peaks at −1.94 and −2.20 V; the second reduction can be ascribed to the reduction of Fe^IFe^0 to Fe^0Fe^0 [40], again shifted to more negative potential compared to complex **1** (−2.11 V). Similarly, complex **4** shows two reduction peaks at −1.88 and −2.10 V. In addition, complexes **2**–**4** each show an irreversible oxidation at +0.28, +0.42, and +0.41 V, respectively, which can be ascribed to the oxidation of Fe^IFe^I to Fe^IFe^{II} [40]. These peaks are negatively shifted by 0.46–0.60 V compared to complex **1**, as observed previously for other phosphine-containing diiron complexes [30, 34, 36].

We further studied the electrocatalytic properties for proton reduction to H_2 catalyzed by complexes **2**–**4** in the presence of acetic acid (0–10 mM). As shown in Figs. 4, 5, and 6, upon addition of 2 mM acetic acid, the first reduction peak is slightly increased but does not grow steadily with sequential addition of more acid. However, new reduction peaks at −2.13, −2.32, and −2.39 V appear and increase significantly with sequential addition of acetic acid. The sharp increase in current intensity suggests an electrocatalytic process for the reduction of protons to H_2 [41, 42].

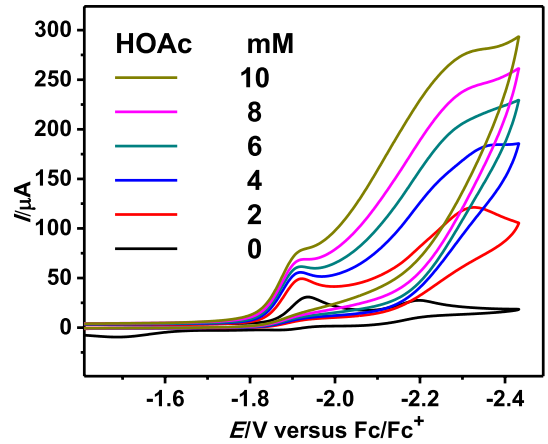

Fig. 5 Cyclic voltammogram of complex **3** (1.0 mM) with HOAc (0–10 mM) in 0.1 M n-Bu_4NPF_6/MeCN at a scan rate of 100 mV s^{-1}

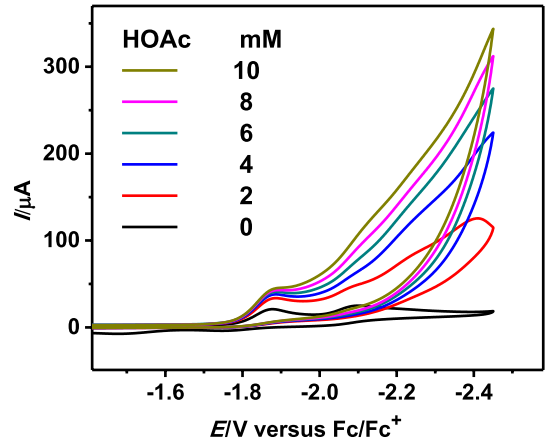

Fig. 6 Cyclic voltammogram of complex **4** (1.0 mM) with HOAc (0–10 mM) in 0.1 M n-Bu_4NPF_6/MeCN at a scan rate of 100 mV s^{-1}

Conclusions

In conclusion, we have presented the synthesis and characterization of three diiron ethane-1,2-dithiolate complexes with monosubstituted phosphine coligands. The X-ray crystal structures of the complexes revealed that they consist of a diiron core with a bridging ethane-1,2-dithiolate ligand, five terminal carbonyls, and an apically coordinated phosphine ligand.

Supplementary material

CCDC 1890166−1890168 contain the supplementary crystallographic data for this paper. These data can be obtained free of charge from The Cambridge Crystallographic Data Centre via www.ccdc.cam.ac.uk/data_request/cif.

Acknowledgements This research was supported by Zhejiang Provincial Natural Science Foundation of China under Grant LY19B020002, National Natural Science Foundation of China under Grant 21501124, Science & Technology Department of Sichuan Province under Grant 2018JY0235, Education Department of Sichuan Province under Grant 18ZA0337, and Sichuan University of Science & Engineering under Grant S201910622022.

References

1. Tard C, Pickett CJ (2009) Chem Rev 109:2245
2. Gloaguen F, Rauchfuss TB (2009) Chem Soc Rev 38:100
3. Lubitz W, Ogata H, Rüdiger O, Reijerse E (2014) Chem Rev 114:4081
4. Rauchfuss TB (2015) Acc Chem Res 48:2107
5. Li Y, Rauchfuss TB (2016) Chem Rev 116:7043
6. Cammack R (1999) Nature 397:214
7. Lemon BJ, Peter JW (1999) Biochemistry 38:12969
8. Frey M (2002) ChemBioChem 3:153
9. Peters JW, Lanzilotta WN, Lemon BJ, Seefeldt LC (1998) Science 282:1853
10. Nicolet Y, Piras C, Legrand P, Hatchikian CE, Fontecilla-Camps JC (1999) Structure 7:13
11. De Lacey AL, Stadler C, Cavazza C, Hatchikian EC, Fernandez VM (2000) J Am Chem Soc 122:11232
12. Fan H, Hall MB (2001) J Am Chem Soc 123:3828
13. Berggren G, Adamska A, Lambertz C, Simmons TR, Esselborn J, Atta M, Gambarelli S, Mouesca JM, Reijerse E, Lubitz W, Happe T, Artero V, Fontecave M (2013) Nature 499:66
14. Lawrence JD, Li H, Rauchfuss TB (2001) Chem Commun 1482
15. Li H, Rauchfuss TB (2002) J Am Chem Soc 124:726
16. Lawrence JD, Li H, Rauchfuss TB, Bénard M, Rohmer MM (2001) Angew Chem Int Ed 40:1768
17. Ott S, Kritikos M, Åkermark B, Sun L, Lomoth R (2004) Angew Chem Int Ed 43:1006
18. Lyon EJ, Georgakaki IP, Reibenspies JH, Darensbourg MY (2001) J Am Chem Soc 123:3268
19. Li P, Wang M, He C, Li G, Liu X, Chen C, Åkermark B, Sun L (2005) Eur J Inorg Chem 2005:2506
20. Song LC, Yan J, Li YL, Wang DF, Hu QM (2009) Inorg Chem 48:11376
21. Capon JF, Hassnaoui SE, Gloaguen F, Schollhammer P, Talarmin J (2005) Organometallics 24:2020
22. Winter A, Zsolnai L, Huttner G (1982) Z Naturforsch 37b:1430
23. Justice AK, Nilges MJ, Rauchfuss TB, Wilson SR, De Gioia L, Zampella G (2008) J Am Chem Soc 130:5293
24. Olsen MT, Bruschi M, De Gioia L, Rauchfuss TB, Wilson SR (2008) J Am Chem Soc 130:12021
25. APEX2, version 2009.7-0, Bruker AXS, Inc., Madison, 2007
26. Sheldrick GM (2001) SADABS: program for absorption correction of area detector frames. Bruker AXS Inc., Madison
27. Dolomanov OV, Bourhis LJ, Gildea RJ, Howard JAK, Puschmann H (2009) J Appl Crystallogr 42:339
28. Sheldrick GM (2008) Acta Crystallogr A 64:112
29. Lian M, He J, Yu XY, Mu C, Liu XF, Li YL, Jiang ZQ (2018) J Organomet Chem 870:90
30. Abul-Futouh H, Almazahreh LR, Harb MK, Görls H, El-khateeb M, Weigand W (2017) Inorg Chem 56:10437
31. Zhao PH, Li XH, Liu YF, Liu YQ (2014) J Coord Chem 67:766
32. Li YL, He J, Wei J, Wei J, Mu C, Wu Y, Xie B, Zou LK, Wang Z, Wu ML, Li HM, Gao F, Zhao PH (2017) Polyhedron 137:325
33. Chen FY, He J, Mu C, Liu XF, Li YL, Jiang ZQ, Wu HK (2019) Polyhedron 160:74
34. Chen XQ, Liu XF, Jiang ZQ, Zhang YX, Li X, Tian XN, Liu XH (2016) J Coord Chem 69:1439
35. Lu DT, He J, Yu XY, Liu XF, Li YL, Jiang ZQ (2018) Polyhedron 149:1
36. Ortega-Alfaro MC, Hernández N, Cerna I, López-Cortéz JG, Gómez E, Toscano RA, Alvarez-Toledano C (2004) J Organomet Chem 689:885
37. He J, Deng CL, Li Y, Li YL, Wu Y, Zou LK, Mu C, Luo Q, Xie B, Wei J, Hu JW, Zhao PH, Zheng W (2017) Organometallics 36:1322
38. Zhao PH, Ma ZY, Hu MY, He J, Wang YZ, Jing XB, Chen HY, Wang Z, Li YL (2018) Organometallics 37:1280
39. Zhao PH, Hu MY, Li JR, Ma ZY, Wang YZ, He J, Li YL, Liu XF (2019) Organometallics 38:385
40. Song LC, Ge JH, Zhang XG, Liu Y, Hu QM (2006) Eur J Inorg Chem 2006:3204
41. Gloaguen F, Lawrence JD, Rauchfuss TB (2001) J Am Chem Soc 123:9476
42. Chong D, Georgakaki IP, Mejia-Rodriguez R, Sanabria-Chinchilla J, Soriaga MP, Darensbourg MY (2003) Dalton Trans 4158